Measurement Science and Technology

PAPER

Image-type displacement measurement resolution improvement without magnification imaging

To cite this article: Hai Yu 2022 *Meas. Sci. Technol.* **33** 015103

IOP Publishing Measurement Science and Technology

Meas. Sci. Technol. **33** (2022) 015103 (7pp) https://doi.org/10.1088/1361-6501/ac2feb

Image-type displacement measurement resolution improvement without magnification imaging

Hai Yu

Changchun Institute of Optics, Fine Mechanics and Physics, Chinese Academy of Sciences, Changchun 130033, People's Republic of China

E-mail: yuhai@ciomp.ac.cn

Received 10 June 2021, revised 3 October 2021
Accepted for publication 14 October 2021
Published 27 October 2021

CrossMark

Abstract
The imaging-type displacement measurement (IDM) technique is better-suited to high-resolution measurement than the traditional moiré fringe technique. In Angular displacement measurement, IDM generally requires lens-magnified imaging processes to reach the proper resolution, which depends on overly large imaging lenses and highly complex, generally unreliable equipment, making the technique not conducive to industrial application. The resolution of an IDM device was improved in this study without the use of an imaging lens. The lensless imaging principle was established, then a new algorithm based on multi-line fusion and denoising was developed to improve the displacement subdivision resolution. The proposed algorithm was verified by both simulation and experimentation. The simulation shows that the proposed algorithm effectively reduces positioning operation noise. In the experiment, an angular measurement resolution of 0.039″ (25-bit) was achieved on a 70 mm diameter circular grating. The proposed method lays a foundation for further high-resolution displacement measurement techniques.

Keywords: displacement measurement, high resolution, lensless imaging, denoising algorithm

(Some figures may appear in color only in the online journal)

1. Introduction

Digital displacement measurement techniques are mainly photoelectric [1, 2], magnetic [3], or capacitive [4, 5]. Among them, photoelectric displacement technology allows for large-range absolute measurement and has strong anti-interference performance. Advanced image processing technology allows for effective digital imaging processes with image detectors equipped to measure angle displacement. Imaging-type displacement measurement (A-IDM) technology serves a novel photoelectric measurement technique wherein the traditional moiré fringe signal is replaced with pixel array information, which makes it easier to achieve high-resolution displacement measurement.

There have been many previous studies on IDM technology. Leviton and Frey [6], for example, used an area array image sensor to receive a grating pattern with reference line and binary code elements in 2003, realizing measurement resolution of 0.01 µm and accuracy of 0.2 µm. Sugiyam *et al* [7] studied used an area array sensor for absolute displacement measurement technology to realize 14-bit angular resolution on a 30 mm diameter circular grating based on code recognition. In 2010, Tresanchez *et al* [8] proposed a image sensor inside an optical mouse to obtain image information, with a microprocessor to calculate and realize angle measurement cost-effectively and at low resolution. Das *et al* [9] proposed a displacement measurement method based on the gray gradient pattern in a 2013 study which achieved a resolution of 1 mm. Baji *et al* [10] proposed a displacement measurement method based on color recognition to reach a linear error of 1° using a code disc coated with uniform color. Kim *et al* [11] realized 13-bit coding recognition on a 41.72 mm diameter grating

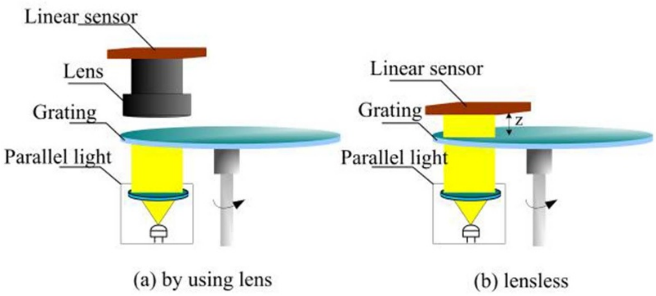

Figure 1. Optical path of imaging-type measurement.

with the phase-shifting coding mode in a micro image detection system; the angle measurement accuracy was 0.044″. Mu *et al* [12] used a CMOS image sensor to recognize single code channel coding and 20-bit coding recognition. Existing measurement methods based on color recognition can achieve absolute measurement, but the measurement resolution is limited. The lack of subdivision algorithm leaves room for further improvement to the resolution of devices based on coding recognition.

Xu *et al* [13] proposed a method of superposing image arrays to form virtual moiré fringes in a 2010 study, reaching a resolution of 0.1 μm and measurement accuracy of 0.4 μm. Fu and Zhang [14] constructed a time grating double coordinate system based on CCD pixels for measurement accuracy of ± 2 μm. Lashmanov *et al* [15] used a camera to collect and measure a scale ruler with scale lines for measurement accuracy of 1.65 μm. Liu *et al* [16] measured displacement based on gray value calculation to reach measurement accuracy of 4 μm by using an imaging lens. The magnifying imaging lens readily achieves high-resolution imaging, but it increases the volume of the device and is easily affected by vibration and virtual focus problems. The measurement accuracy of these devices is not sufficient; there is still demand for new, high-precision displacement measurement algorithms.

Existing imaging-type measurement technologies require magnified imaging to achieve high resolution. Previously established image displacement measurement techniques mainly include optical paths based on imaging lenses or lensless imaging, as shown in figure 1.

The optical path based on the imaging lens is shown in figure 1(a). The imaging lens enlarges the pattern on the grating code disk, then is collected by the image sensor to complete the displacement measurement. Magnifying imaging does provide high-resolution measurement but the volume of the device is excessively large and the optical path is overly complex.

The optical path with lensless imaging is shown in figure 1(b). The image sensor in this device is placed close to the grating. A parallel light source irradiates the grating encoder, then the pattern on the grating is mapped to the image sensor. This method can be applied in smaller, more reliable devices than lens-based imaging, but its measurement resolution needs improvement.

In a previous study, we used lensless imaging to achieve resolution of 0.62″ and accuracy of 12.93″ on a 38 mm diameter code disk [17]. In order to further improve the resolution, we developed a super-resolution algorithm using pixel differences to achieve resolution of 0.15″ on a 38 mm diameter code disk [18]. It is possible—and indeed necessary, to secure effective devices based on this technology—to further improve the measurement resolution.

First, as discussed in detail below, we established an location algorithm based on multi-line fusion. We then built an n-order denoising algorithm based on the multiple acquisition method and the mean value. Finally, we applied the algorithm to a circular grating with a diameter of 70 mm to achieve a stable output of 25-bit measurement resolution.

The rest of this paper is organized as follows. Section 2 describes the image displacement measurement principle. Section 3 presents the proposed location and denoising algorithm. Section 4 reports our simulation results and section 5 gives our experimental results. Section 6 provides a brief summary and conclusion.

2. Principle of image displacement measurement technology

2.1. Measurement principle

The A-IDM technology discussed here includes a linear image sensor that collects marking lines on the circular grating followed by absolute displacement measurement. When no imaging lens is used, the image sensor must be placed near to the grating to realize projection imaging. The measurement principle is shown in figure 2.

As shown in figure 2, the light emitted by the parallel light source irradiates the calibration grating and projects onto the image sensor. We set the distance between the image sensor and the grating as $z \leqslant 1$ mm to improve the imaging quality. The sensor collected the image of grating is called the image detection area (IDA).

To realize absolute coding, the width of the lines in the IDA were divided into 'wide' and 'narrow' categories with coding values of '1' and '0', respectively. The encoding values represented by all lines in the circle will be encoded in the m-sequence pseudo-random encoding mode. By arranging the positions of wide and narrow lines reasonably, we could realize a maximum of 2^N codes in the circle. Absolute decoding can then be realized by identifying the marking lines.

2.2. Code recognition

When we recognized and decoded the encoded lines on the grating, we only needed to judge the 'width' and 'narrowness' of each line in IDA to obtain the encoded value. The decoding value of the current position can be obtained by looking it up in the decoding table. The code recognition principle is shown in figure 3.

According to figure 3, when the number of coded lines is $m = 9$-bit, the image collected by the image sensor contains nine coded lines, at least. The recognized coding group in figure 3 is $\{0, 1, 0, 0, 1, 1, 1, 1, 1\}$. We can get the decoding value D according to the decoding lookup table.

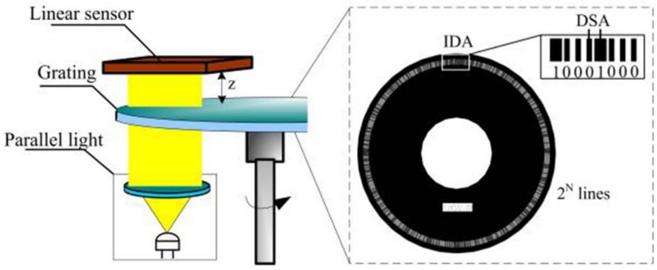

Figure 2. Grating projection measurement method.

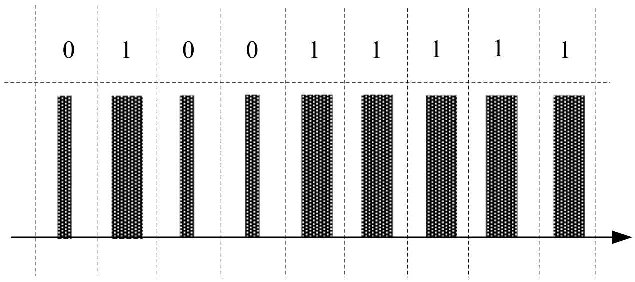

Figure 3. Coding recognition principle.

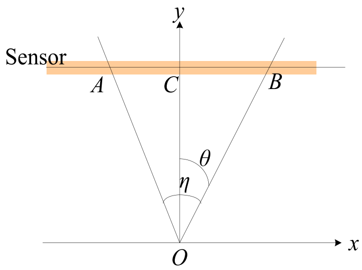

Figure 4. Displacement subdivision area (DSA).

2.3. Subdivision algorithm

The displacement subdivision area (DSA) in the IDA was subdivided as per the calculation principle shown in figure 4.

As shown in figure 4, point C is the midpoint of the image collected by the linear image sensor (this point is preset). We set the angle between the two coding lines on both sides of point C to $\eta = 2\pi/2^N$. The image sensor and two coding lines intersect at point A and point B. When the η angle is small, the ratio between θ and η is approximately equal to the ratio between CB to AB. The subdivision algorithm is:

$$S = \frac{\theta}{\eta} \cdot 2^m \approx \frac{CB}{AB} \cdot 2^m \tag{1}$$

where 2^m is the quantized value of the η angle. A larger 2^m results in a higher resolution.

In summary, after Code recognition and Subdivision operation, A-IDM measurement results can be expressed as:

$$O = D \cdot 2^m + S \tag{2}$$

where, O is the final measured value, D is decoding value is section 2.2.

In addition, equation (1) also shows that because the subdivision algorithm is a ratio, the key to improving resolution is to improve the positioning accuracy of point A and point B.

3. Location and denoising of coding lines

3.1. Multi-line fusion algorithm

According to the subdivision algorithm (equation (1)), it is necessary to improve the resolution of positioning points to improve the A-IDM resolution. We developed a multi-line fusion algorithm to remove the noise from a single image and improve the coded line positioning accuracy. When 2^9 coding lines are included in the circle of the grating code disk, the image collected by the image sensor is as shown in figure 5.

As shown in figure 5, the DSA is composed of two lines a_4 and a_5 on either side of the image center. According to the subdivision algorithm (equation (1)), as mentioned above, the key to subdivision is to accurately locate the intersection points A and B.

The collected image contains noise which affects the positioning accuracy. The traditional approach involves directly using the centroid algorithm to locate the a_4 and a_5 marking lines. However, due to the small range of a_4 and a_5 in the image, noise has a significant impact on the positioning accuracy. To remedy this, we propose a location algorithm based on the multi-line fusion algorithm.

We first used the square weighted centroid algorithm to calculate the centroids $x_{a1} \sim x_{a8}$ of $a_1 \sim a_8$:

$$x_a = \frac{\sum\limits_{x \in P} x \cdot p'(x)^2}{\sum\limits_{x \in P} p'(x)^2} \tag{3}$$

where x_a is the location of each line, $p'(x)$ is the gray value after the super-resolution operation, and P is the range of each line. The range of P can be determined by threshold comparison.

Next, we summed and took the mean value for the lines with a_4 and a_5 as symmetrical. The lines with x_{a4} as the center symmetry are $\{x_{a3}, x_{a5}\}$, $\{x_{a2}, x_{a6}\}$, $\{x_{a1}, x_{a7}\}$ in this case and the lines with x_{a5} as the center symmetry are $\{x_{a4}, x_{a6}\}$, $\{x_{a3}, x_{a7}\}$, $\{x_{a2}, x_{a8}\}$. After fusion, the positions of A and B are:

$$A = \frac{(x_{a3} + x_{a5}) + (x_{a2} + x_{a6}) + (x_{a1} + x_{a7}) + x_{a4}}{7} \tag{4}$$

$$B = \frac{(x_{a4} + x_{a6}) + (x_{a3} + x_{a7}) + (x_{a2} + x_{a8}) + x_{a5}}{7} \tag{5}$$

where $x_{a1} \sim x_{a8}$ are the centroids of $a_1 \sim a_8$, respectively. For subdivision calculation of the displacement, the fused location points are introduced into equation (1) to obtain the subdivision value. The mean algorithm effectively reduces the noise interference in the image during the fusion process.

3.2. Denoising algorithm

The acquired image contains some noise, which will affect the measurement resolution. Because the noise of the sampling

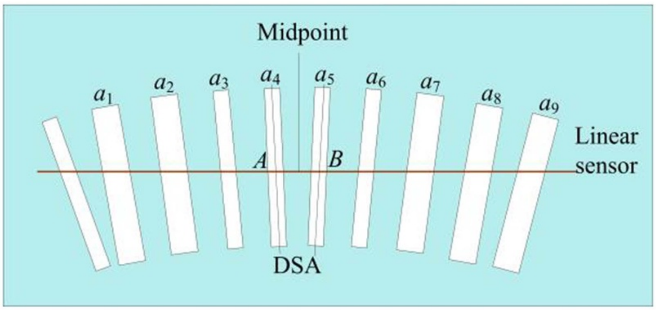

Figure 5. Subdivision algorithm schematic.

results at different time points is randomly distributed, point A in the DSA can be set to be $A(i)$ in the ith location. During each measurement iteration, the current positioning value is recorded as $A(i)$. $AA(i-n) \sim AA(i-1)$ is the value after the denoising operation. If $i = 1$ initially, then $AA(1n) = A(1)$, $AA(1n+1) = A(1),\ldots, AA(0) = A(1)$, while n is the preset positive integer. The denoising algorithm can be expressed as:

$$AA(i) = \frac{A(i) + AA(i-1) + \ldots + AA(i-n)}{n+1} \tag{6}$$

where $AA(i)$ is the value after the denoising operation. Equation (6) is an n-order denoising algorithm which can effectively suppress noise in the acquisition circuit because it takes a mean value. Equation (6) can also be used to denoise point B in the DSA and to obtain the value $BB(i)$ of point $B(i)$. After denoising, the subdivision operation can be conducted according to equation (1): $S = \eta(BB - C)/(BB - AA)$.

We made $n = 5$ to realize a 5th order denoising algorithm. Equation (6) affected the measurement frequency response at this point. Due to high-speed movement, the resolution requirement was low in our case; the measurement resolution requirement is strict at lower speeds. To satisfy the dynamic measurement requirements and improve the measurement frequency response, we only added the denoising algorithm when the image sensor moved at a low speed so as to ensure the proper high-speed measurement frequency response.

According to a previous study [14], when using the super-resolution interpolation algorithm, 23-bit resolution can be achieved on a 38 mm diameter grating; this can be converted to a resolution of $(38\ \text{mm} \times 3.14)/2^{23} \approx 0.015\ \mu\text{m}$. In the denoising operation, we judged the difference between the measuring output $O(i)$ and $O(i-1)$. That is, $\Delta O = |O(i) - O(i-1)|$. If $\Delta O < 2 \times 0.015\ \mu\text{m}$, the operation in equation (6) was added; if $\Delta O \geqslant 2 \times 0.015\ \mu\text{m}$, it was not added. The resolution could be further improved in this way without affecting the measurement frequency response.

4. Simulation

We tested the performance of the proposed localization and denoising algorithm by operating a simulated image sensor in MATLAB software. We set 1000 images in total with resolution of 1×512 pixels; the gray value of translucent position was set to 1000 and the light-proof part as 0. The pixel number and gray value were preset as there is no fixed standard.

According to previous studies, we added random noise with 2% of the maximum gray value ($1000 \times 2\% = 20$) to the image. The result is shown in figure 6(a).

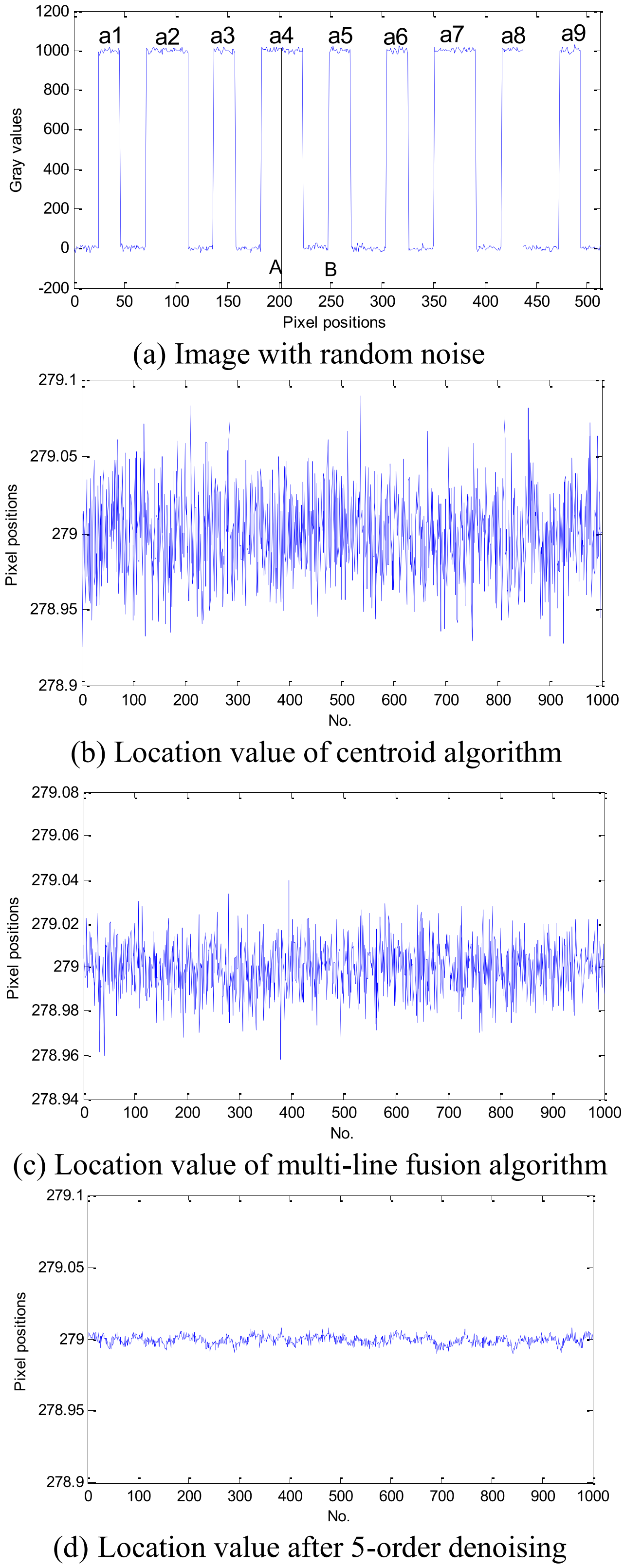

Figure 6. Test after adding random noise.

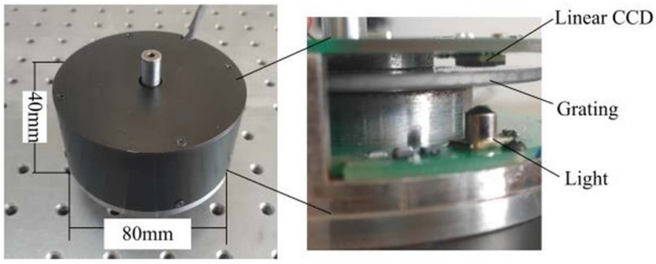

Figure 7. Experimental device.

We conducted locating and de-noising operations using the a_5 line in this simulation. The fluctuation curve of the positioning curve based on the gray value square weighted centroid algorithm is shown in figure 6(b), where the mean square deviation of the fluctuation is 0.0247 pixels. The wave curve of positioning after adding the multi-line fusion algorithm is shown in figure 6(c), where the mean square deviation is 0.0118 pixels. The fluctuation curve of the positioning after adding the five-order denoising algorithm is shown in figure 6(d), where the mean square deviation is 0.0028 pixels.

As shown, the noise of the positioning value was effectively suppressed when the multi-line fusion algorithm and five-order denoising algorithm were added simultaneously.

5. Experiments

We designed an experimental device (figure 7) to further test the performance of the proposed algorithm.

The height of the experimental device is 40 mm and the outer diameter is 80 mm. The diameter of the grating code disk is 70 mm and there are $2^9 = 512$ coding lines in the circumference of the grating. The resolution of the linear image sensor is 1×512 pixels and the pixel interval $\Delta x = 7.9375$ µm.

5.1. Positioning experiment

We fixed the principal axis of the device so that the grating encoder and linear image sensor were relatively stationary during the experiment. The a_5 line in the collected image was located, then the location results were collected 1000 times continuously. The results are shown in figure 8.

The positioning calculation result with mean square deviation of 0.0018 pixels is shown in figure 8(b). The pixel interval after the super-resolution algorithm was $\Delta x = 7.9375$ µm, so the displacement caused by fluctuation was $0.0018 \cdot \Delta x = 0.014$ µm. This value is consistent with the 23-bit resolution achieved on a 38 mm diameter grating in a previous study [10].

After adding the multi-line fusion algorithm, the calculated positioning value was as shown in figure 8(c). The mean square deviation of the fluctuation is 0.000 11 pixels. In effect, the multi-line fusion algorithm can successfully suppress noise.

The results of multi-scale fusion after operating the five-order denoising algorithm are shown in figure 8(d), where the standard deviation is 0.0006 pixels. The noise of the location value was significantly reduced in this case and the stability was improved when the multi-line fusion algorithm and the

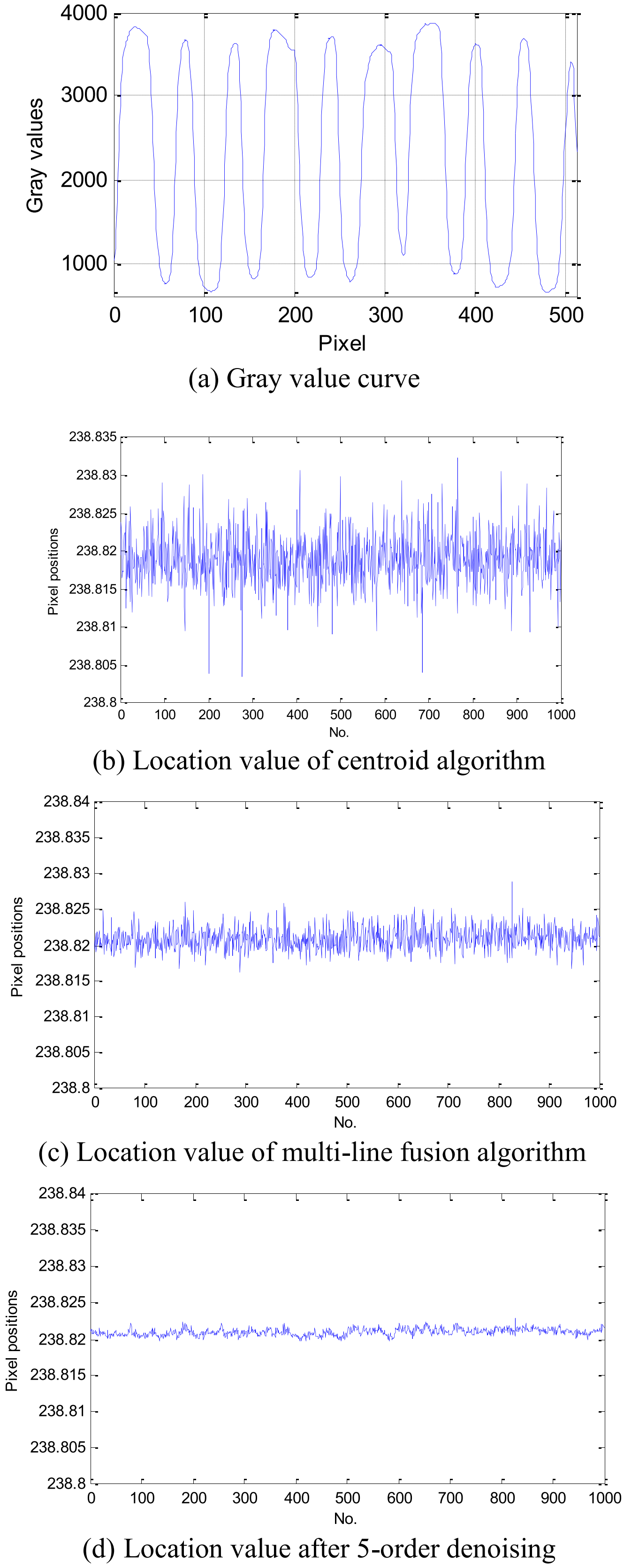

Figure 8. Numerical curve of marking positioning.

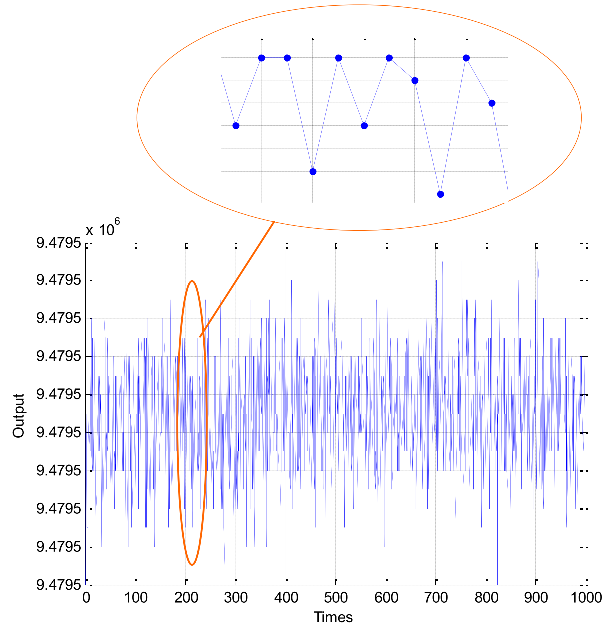

(a) Output without denoising algorithm (1 resolution per grid)

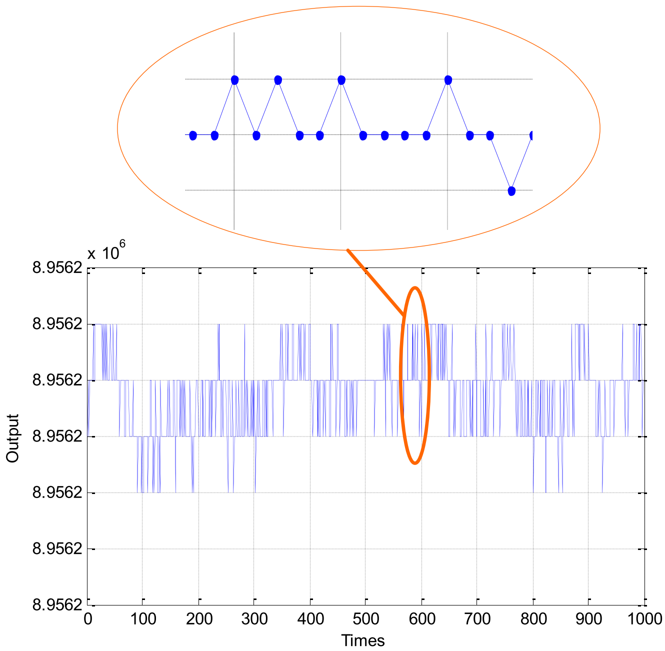

(b) Output of denoising location algorithm (1 resolution per grid)

Figure 9. Resolution test.

five-order denoising algorithm were used at the same time versus applying them separately.

We multiplied the mean square deviation in figure 8(d) by the pixel interval as $0.0006{\cdot}\Delta x = 0.0047$ µm. The circumference of the grating code disc with a diameter of 70 mm is $70 \times 3.14 = 219.8$ mm. When there is a noise fluctuation of 0.0047 µm, within the circumference of the grating code disc, at least the measurement

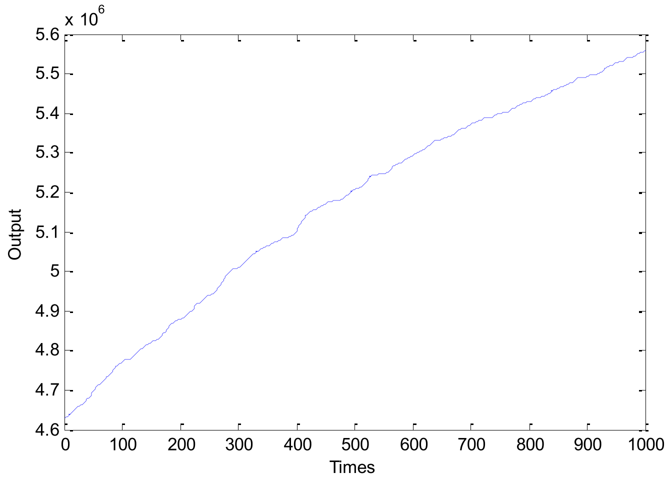

Figure 10. Resolution test.

resolution of $70 \times 3.14/2^{25} = 0.0065$ µm can be guaranteed (0.0065 µm > 0.0047 µm). In other words, 25-bit measurement resolution can be achieved.

By this, we set $2^m = 2^{16}$ in equation (1). Because there are $2^N = 2^9$ lines in the circumference of the grating code disk, the measurement resolution is $360°/2^{9+16}$. That is, 25 bit measurement resolution.

5.2. Resolution stability experiment

'Resolution stability' refers to the fluctuation of the output displacement measurement value when the spindle of the angular displacement measuring device is fixed. We imposed $2^m = 2^{16}$ in the subdivision algorithm. The grating circle we used contains $2^N = 2^9$ lines, so we synthesized a measurement resolution of 25-bit. The output values (1000 iterations) based on the rotating axis of the experimental result are shown in figure 9. Due to the high 25-bit resolution, the spindle was weak in this test. We were able to judge whether the measurement was effective by observing the binary carry of the output values.

When the denoising algorithm was not added, the fluctuation of the output value was as shown in figure 9(a). The output values were not carried one-by-one in this case. The jumping range exceeded one resolution occasionally, even reaching six resolutions. This suggests that the output values contained error, so the resolution of 25-bit could not be achieved. The fluctuation curve of the output values after adding the denoising and positioning algorithm is shown in figure 9(b). The output value carried one resolution every time with no skip or error codes. Thus, a resolution of 25-bit was effectively achieved.

We next rotated the axis slowly and collected the angle values of 1000 output times, as shown in figure 10. As the output data increased from 4628 722 to 5556 481, the output value was carried forward without any error codes. Therefore, the 25-bit resolution achieved by the device was correct when rotating throughout the entire test.

Compared with the 23-bit resolution achieved by previous researchers [18], the 25-bit resolution we achieved using the proposed algorithm represents a significant improvement.

6. Conclusion

This paper proposed a measurement method based on multi-line fusion and an n-order denoising algorithm. We established an location algorithm based on multi-line fusion, then built an n-order denoising algorithm based on the multiple acquisition and mean value. We conducted simulation and experimental analyses to validate the proposed method.

Our simulation results show that the proposed algorithm effectively reduces the noise from image acquisition and improves the positioning stability. In an experimental device, we achieved measurement resolution of $0.039''$ (25-bit) on a 70 mm grating. Compared with our previous work (23-bit resolution on 38 mm diameter grating), the algorithm we developed in this study significantly improves the measurement resolution.

When applying the multi-line fusion and n-order descending algorithm together, increasing the order of n reduces fluctuations in the positioning value during measurement, which effectively improves the measurement resolution. A larger n value creates a more obvious denoising effect, but also drives down the response speed of the displacement measurement process. The order of n needs to be selected carefully during any practical application of the proposed method.

The performance of A-IDM techniques can be significantly improved by enhancing the resolution. The method proposed in this paper lays a foundation for further research on high-resolution A-IDM technology.

Data availability statement

No new data were created or analyzed in this study.

Funding

This project is supported by the National Natural Science Foundation of China (Grant Nos. 52075520 and 51605465), Science and Technology Development Programme of Jilin Province (Grant No. 20210201097GX)

ORCID iD

Hai Yu https://orcid.org/0000-0001-7679-735X

References

[1] Hane K, Endo T, Ishimori M and Sasaki M 2002 Integration of grating-image-type encoder using Si micromachining *Sens. Actuators* A **97** 139–46

[2] Liu F, Wang W, Wang L and Feng P 2013 Error analyses and calibration methods with accelerometers for optical angle encoders in rotational inertial navigation systems *Appl. Opt.* **52** 7724–31

[3] Zhang Z, Ni F, Dong Y, Jin M and Liu H 2013 A novel absolute angular position sensor based on electromagnetism *Sens. Actuators* A **194** 196–203

[4] Pu H, Liu H, Liu X, Peng K and Yu Z 2018 A novel capacitive absolute positioning sensor based on time grating with nanometer resolution *Mech. Syst. Signal Process.* **104** 705–15

[5] Zhang D, Zhao S, Zheng Q and Lin L 2019 Absolute capacitive grating displacement measuring system with both high-precision and long-range *Sens. Actuators* A **295** 11–22

[6] Leviton D B and Frey B J 2003 Ultra-high resolution, absolute position sensors for cytostatic applications *Proc. SPIE* **4850** 776–87

[7] Sugiyam Y, Matsu Y, Toyod H, Mukozaka N, Ihori A, Abe T, Takabe M and Mizuno S 2008 A 3.2 kHz 14-bit optical absolute rotary encoder with a CMOS profile sensor *IEEE Sens. J.* **8** 1430–6

[8] Tresanchez M, Pallejà T, Teixidó M and Palacín J 2010 Using the image acquisition capabilities of the optical mouse sensor to build an absolute rotary encoder *Sens. Actuators* A **157** 161–7

[9] Das S, Sarkar T S and New A 2013 Method of linear displacement measurement utilizing grayscale image *Int. J. Electron. Electr. Eng.* **1** 176–81

[10] Baji J S, Stupara D Z, Dakić B M, Živanov M B and Nagy L F 2014 An absolute rotary position sensor based on cylindrical coordinate color space transformation *Sens. Actuators* A **213** 27–34

[11] Kim J A, Kim J W, Kang C S, Jin J and Eom T B 2016 Absolute angle measurement using a phase-encoded binary graduated disk *Measurement* **80** 288–93

[12] Mu Y, Jiang J, Ding N, Ni Q and Chang Y 2019 A 7.4 kHz, 20-bit image encoder with a CMOS linear image sensor *Opt. Quantum Electron.* **51** 321

[13] Xu J, Ye W, Ni X and Cao X 2010 Virtual moiré fringe for grating measurement system based on CMOS microscopic imaging *Proc. SPIE* **7853** 785325

[14] Fu M and Zhang X 2015 Study on the time-grating sensor method of the static light field type based on timing-driven *Appl. Mech. Mater.* **3468** 1409–13

[15] Lashmanov O U, Vasilev A S, Vasileva A V, Anisimov A G and Korotaev V V 2018 High-precision absolute linear encoder based on a standard calibrated scale *Measurement* **123** 226–34

[16] Liu X, Hu J, Tong H, Ge A, Du S and Zhu Y 2019 Linear displacement measurement based on image grayscale information *Acta Opt. Sin.* **39** 191–7 (In Chinese)

[17] Yu H, Wan Q, Lu X, Zhao C and Du Y 2018 A robust sub-pixel subdivision algorithm for image-type angular displacement measurement *Opt. Laser Eng.* **100** 234–8

[18] Yu H, Jia X, Wan Q, Zhao C and Sun Y 2020 High-resolution angular measurement arithmetic based on pixel interpolations *Measurement* **149** 106948